ORIGINAL PAPER

The EMT transcription factor ZEB1 blocks osteoblastic differentiation in bone development and osteosarcoma

Manuel Ruh[1][†], Marc P Stemmler[1][†], Isabell Frisch[1], Kathrin Fuchs[1], Ruthger van Roey[1], Julia Kleemann[1], Maike Roas[1][‡], Harald Schuhwerk[1], Rebecca L Eccles[1], Abbas Agaimy[2], Daniel Baumhoer[3], Geert Berx[4,5], Fabian Müller[6], Thomas Brabletz[1,7][§][*] and Simone Brabletz[1][§][*]

[1] Department of Experimental Medicine 1, Nikolaus-Fiebiger-Center for Molecular Medicine, Friedrich-Alexander-University Erlangen-Nürnberg, Erlangen, Germany
[2] Institute of Pathology, Friedrich-Alexander-University Erlangen-Nürnberg, Erlangen, Germany
[3] Bone Tumor Reference Centre, Institute of Pathology, University Hospital and University of Basel, Basel, Switzerland
[4] Cancer Research Institute Ghent (CRIG), Ghent University, Ghent, Belgium
[5] Molecular and Cellular Oncology Laboratory, Department of Biomedical Molecular Biology, Ghent University, Ghent, Belgium
[6] Department of Medicine 5 for Hematology and Oncology, Friedrich-Alexander-University Erlangen-Nürnberg, Erlangen, Germany
[7] Comprehensive Cancer Center Erlangen-EMN, Erlangen University Hospital, Friedrich-Alexander-University Erlangen-Nürnberg, Erlangen, Germany

*Correspondence to: S Brabletz or T Brabletz, Department of Experimental Medicine 1, Nikolaus-Fiebiger-Center for Molecular Medicine, Friedrich-Alexander-University Erlangen-Nürnberg, Glückstrasse 6, 91054 Erlangen, Germany.
E-mail: simone.brabletz@fau.de or thomas.brabletz@fau.de

[†]Equal first authors.
[§]These authors contributed equally to this work.
[‡]Department of Medicine III, University Hospital, LMU München, Germany

Abstract

Osteosarcoma is an often-fatal mesenchyme-derived malignancy in children and young adults. Overexpression of EMT-transcription factors (EMT-TFs) has been associated with poor clinical outcome. Here, we demonstrated that the EMT-TF ZEB1 is able to block osteoblastic differentiation in normal bone development as well as in osteosarcoma cells. Consequently, overexpression of ZEB1 in osteosarcoma characterizes poorly differentiated, highly metastatic subgroups and its depletion induces differentiation of osteosarcoma cells. Overexpression of ZEB1 in osteosarcoma is frequently associated with silencing of the imprinted *DLK–DIO3* locus, which encodes for microRNAs targeting ZEB1. Epigenetic reactivation of this locus in osteosarcoma cells reduces ZEB1 expression, induces differentiation, and sensitizes to standard treatment, thus indicating therapeutic options for ZEB1-driven osteosarcomas.
© 2021 The Authors. *The Journal of Pathology* published by John Wiley & Sons, Ltd. on behalf of The Pathological Society of Great Britain and Ireland.

Introduction

Osteosarcoma, the most common primary bone cancer, particularly affects children and adolescents. Osteosarcoma is a leading cause of cancer-related death in young adults. This is mainly due to the early spread of tumor cells to the lung, the most prevalent site of metastasis in osteosarcoma patients [1]. Defective osteogenic differentiation seems to be an important feature of osteosarcoma tumorigenesis and may explain its high malignant potential [2]. However, the causative molecular mechanisms are not fully understood.

Aberrant activation of the epithelial–mesenchymal transition (EMT) program is widely accepted to be a major driver of tumor progression in epithelial-derived malignancies but plays a role in non-epithelial tumors as well [3,4]. In this regard, overexpression of EMT-transcription factors (EMT-TFs), including zinc finger E-box-binding homeobox 1 (ZEB1), was associated with increased invasion and proliferation of osteosarcoma cells and poor clinical outcome in osteosarcoma [5–9]. In many younger osteosarcoma patients, the *DLK1–DIO3* locus exhibits imprinting defects. Resulting downregulation of miRNAs encoded therein correlates with shorter overall survival and metastasis [10–13]. The imprinted *DLK1–DIO3* locus represents the largest miRNA cluster in mammals, including 52 different miRNAs [14], of which several have already been shown to target core EMT-TFs including ZEB1 [8,15–18]. Thus, silencing of *DLK–DIO3* might be involved in ZEB1 overexpression in osteosarcoma.

In this study, amongst the core EMT-TFs, we selectively observed a clinically relevant upregulation of ZEB1 in

osteosarcoma and demonstrated its crucial role in controlling differentiation in normal osteoblast development and maintaining an undifferentiated state of osteosarcoma cells. Epigenetic reactivation of *DLK1-DIO3*-encoded microRNAs reduces ZEB1 expression and induces differentiation and chemotherapeutic susceptibility in osteosarcoma cells, indicating a therapeutic strategy for ZEB1-driven osteosarcoma.

Materials and methods

Cell culture

Mouse and human mesenchymal stem cells were cultured in αMEM with 10% FBS and 1% penicillin–streptomycin stock solution. All cell lines were cultivated in DMEM with 10% FBS. Stably transduced cells were cultured and selected using 5 µg/ml puromycin (Sigma-Aldrich, Taufkirchen, Germany; P8833).

Molecular cloning

To analyze the direct regulation of *ZEB1* by miRNAs, the full-length *ZEB1* 3'-UTR was cloned into the pMIR-REPORT™ Luciferase plasmid vector (Thermo Fisher, Waltham, MA, USA; Cat # AM5795). Site-directed mutagenesis was performed to erase miRNA binding sites in the *ZEB1* 3'-UTR. Cloning and mutagenesis were verified by sequencing.

Virus transduction

Cells were transduced with a multiplicity of infection (MOI) of 1 overnight. Cells transduced with virus containing GFP were checked for transduction efficiency by flow cytometry.

For recombination *in vitro*, mMSCs isolated from *ZEB1*^*flox/flox* [19] or *R26-Zeb1*^*tg/tg* mice [20] were transduced with adeno-Cre virus [21] added to the culture medium. Recombination efficiency was determined by genotyping PCR and immunofluorescence analysis.

Transfection of pre-miRNAs and miRNA inhibitors

Transfection of pre-miRNAs or miRNA inhibitors (designed as described in ref 22) was performed 24 h after cell seeding with Lipofectamine RNAiMAX (Thermo Fisher; 13778100) according to the manufacturer's protocol. RNA and protein isolation was performed after 24 h (pre-miRNAs) or 72 h (miRNA inhibitors). Details of the pre-miRNAs and miRNA inhibitors are provided in supplementary material, Table S1.

Differentiation

Osteoblastic differentiation was induced by osteogenic differentiation medium [αMEM, 10% FBS, 1% penicillin–streptomycin stock solution, 200 µM L-ascorbic acid 2-phosphate (Sigma-Aldrich; A8960), 10 mM β-glycerophosphate (Sigma-Aldrich; G9422)]. To analyze early osteoblastic differentiation, the alkaline phosphatase activity was determined. Terminal osteoblastic differentiation was analyzed via staining of calcium deposits with Alizarin red S (Sigma-Aldrich; A5533).

Clonogenic capacity

To assess clonogenic capacity, cells were seeded sparsely in DMEM, 10% FBS. Colonies were fixed with 4% formaldehyde after 8 (143B), 14 (MG-63, hMSC_1) or 21 days (Saos-2); stained with 0.5% crystal violet solution; and counted.

Proliferation assays

Proliferation was assessed using an MTT-based cell viability assay [thiazolyl blue tetrazolium bromide (Sigma-Aldrich; M2128)] according to the manufacturer's protocol.

Drug treatment (*in vitro*)

A dose–response matrix for cancer cells, treated with 5-Aza (Sigma-Aldrich, A3656) and doxorubicin (Sigma-Aldrich; 44583), was generated by adding drugs (day 0) in different dose combinations (5-Aza: 0.256–10 µM; doxorubicin: 3.125–800 nM). The relative cell viability for each drug combination was determined after 3 days relative to day 0 and relative to the untreated control, using an MTT assay (see above). Values were converted into % inhibition and the excess over highest single agent (HSA) was calculated according to the formula: $y_{HSA} = \max(y_1, y_2)$, where y_1 and y_2 represent the effects of corresponding monotherapy.

Western blot analysis

For standard western blotting, the following primary antibodies were used: ACTB (Sigma-Aldrich; A5441, 1:5000); BGLAP (Santa Cruz Biotechnology, Dallas, TX, USA; sc-30044, 1:500); HA (Roche, Mannheim, Germany; 12158167001, 1:500); RUNX2 (Cell Signaling Technology, Danvers, MA, USA; 12556, 1:5000); and ZEB1 (Sigma; HPA027524, 1:5000). Relative protein quantification was conducted using ImageLab (Bio-Rad, Hercules, CA, USA).

RT–qPCR

Total RNA was isolated and reverse transcription performed. cDNA was amplified using Power SYBR Green PCR master mix (mRNA and lncRNA) (Thermo Fisher; 4367659) or ExiLENT SYBR Green master mix (miRNA) (Exiqon, Woburn, MA, USA; 203421). Samples were run in triplicates and normalized to *ACTB*. Primer sequences are listed in supplementary material, Table S2.

Methylation-specific PCR

Methylation of MEG3-DMR was analyzed as described previously [23].

Lung/liver colonization

All mouse experiments were approved by the Committee on Ethics of Animal Experiments of the State of Bavaria (Regierung Unterfranken, Würzburg) and performed according to European Animal Welfare laws and guidelines.

1×10^5 cells in 200 µl of PBS were injected i.v. in NSG mice. After 3 weeks, the mice were sacrificed and GFP-fluorescence images of the lungs/livers were acquired *ex vivo*. For *in vivo* drug treatment, 2×10^5 cells were injected i.v. in NSG mice. Vehicle, doxorubicin (5 mg/kg or 2.5 mg/kg), and 5-Aza (3 mg/kg) were administered by intraperitoneal injections as depicted. On day 16, the mice were sacrificed and GFP-fluorescence images of the lungs were acquired *ex vivo*. Subsequently, lungs were fixed in 4% paraformaldehyde (PFA), embedded in paraffin, sectioned, and stained with Mayer's hematoxylin and eosin solution G (H&E).

Skeletal staining

Zeb1$^{del/+}$ mice were generated by crossing *Zeb1*$^{flox/flox}$ mice [19] with *Sox2*::Cre mice [24]. Embryos at E15.5 were isolated and fixed in 95% ethanol for 24 h. Cartilage was stained for 24 h with Alcian blue. Calcification of bones was detected using Alizarin red S.

Immunohistochemistry

To estimate the differentiation state of osteosarcoma tumor samples, H&E staining on paraffin-embedded tissue sections was performed. ZEB1, SNAI1, and TWIST1 immunohistochemistry (anti-ZEB1, Sigma-Prestige, HPA027524, 1:1000; anti-SNAIL, Cell Signaling Technology, 3879, 1:50; anti-TWIST1, Abcam, Cambridge, UK; ab50581, 1:100) was performed as previously described [25]. Samples were used in accordance with ethical guidelines for the use of retrospective tissue samples provided by the local ethics committee of the FAU Erlangen-Nürnberg (ethics committee statements 24.01.2005). Ethical approval for the TMA cases was given by the ethics committee Basel (reference 274/12).

Gene expression data analysis

mRNA and miRNA expression and survival data of the gene expression microarrays: GSE32981 [26], GSE21257, and GSE69524, were obtained from the Gene Expression Omnibus database (https://www.ncbi.nlm.nih.gov/geo/) and analyzed using GEO2R (https://www.ncbi.nlm.nih.gov/geo/geo2r/) and Microsoft Excel. mRNA expression data of the E-MEXP-3628 microarray data set were downloaded from the ArrayExpress database (https://www.ebi.ac.uk/arrayexpress/) and analyzed using Microsoft Excel. Kaplan–Meier curves were based on the log$_2$ values of the corresponding EMT-TF, which were used to categorize the samples into low (lower third, $n = 18$) or high (upper two-thirds, $n = 35$) expression.

miRNA prediction

Prediction analysis of *ZEB1* 3'-UTR-targeting miRNAs was carried out using online miRNA prediction tools: TargetScan (http://targetscan.org), miRanda (http://microrna.org) [27], and miRDB (http://miRDB.org).

Statistical analysis

Statistical analysis was performed using GraphPad Prism (GraphPad Software, San Diego, CA, USA). All data are depicted as mean $\pm$ SD, unless otherwise specified. The significance between two groups was determined by an unpaired two-tailed Student's *t*-test (parametric) or an unpaired two-tailed Mann–Whitney test (nonparametric). The significance between more than two groups was determined by a one-way ANOVA with correction for multiple comparisons using Dunnett's method (parametric, comparison to one control group) or Tukey's method (parametric, comparison between all groups). Proliferation data were tested for significance using multiple *t*-tests with correction for multiple comparisons using the Holm–Sidak method. Survival data were analyzed with the log-rank (Mantel–Cox) test. Statistical significance is presented as *$p < 0.05$, **$p < 0.01$, ***$p < 0.001$, and ****$p < 0.0001$.

Detailed descriptions of individual methods are provided in supplementary material, Supplementary materials and methods.

Results

ZEB1 is downregulated upon osteoblast differentiation

EMT-TFs are reported to play a role in osteosarcoma. To assess their differential role in osteosarcoma progression, we performed a comparative mRNA expression and survival analysis using publicly available data sets of primary human osteosarcomas. Remarkably, among the five core EMT-TFs (*SNAI1*, *SNAI2*, *ZEB1*, *ZEB2*, and *TWIST1*) [4], only *ZEB1* was considerably elevated in osteosarcoma tumor samples relative to non-neoplastic bone tissues (Figure 1A and supplementary material, Figure S1A) and tended to be upregulated in established distant metastasis compared with primary osteosarcomas, in particular with the non-metastatic tumors (Figure 1B and supplementary material, Figure S1B). Patients with high *ZEB1* expression in their tumor showed a significantly shorter overall survival, but no significant differences in the survival probability were detectable for the other core EMT-TFs (Figure 1C). Furthermore, in human osteosarcoma cell lines (hOSCs), ZEB1 protein levels were consistently elevated compared with non-neoplastic bone marrow-derived human mesenchymal stem cells (hMSCs) (supplementary material, Figure S1C), which can give rise to osteosarcomas and are the direct precursors of committed pre-osteoblasts, the considered cellular origin of osteosarcoma [28,29]. Interestingly, *in vitro* differentiated osteoblasts, validated by an increased expression of osteoblastic marker genes and acquired Alizarin red-stained calcium
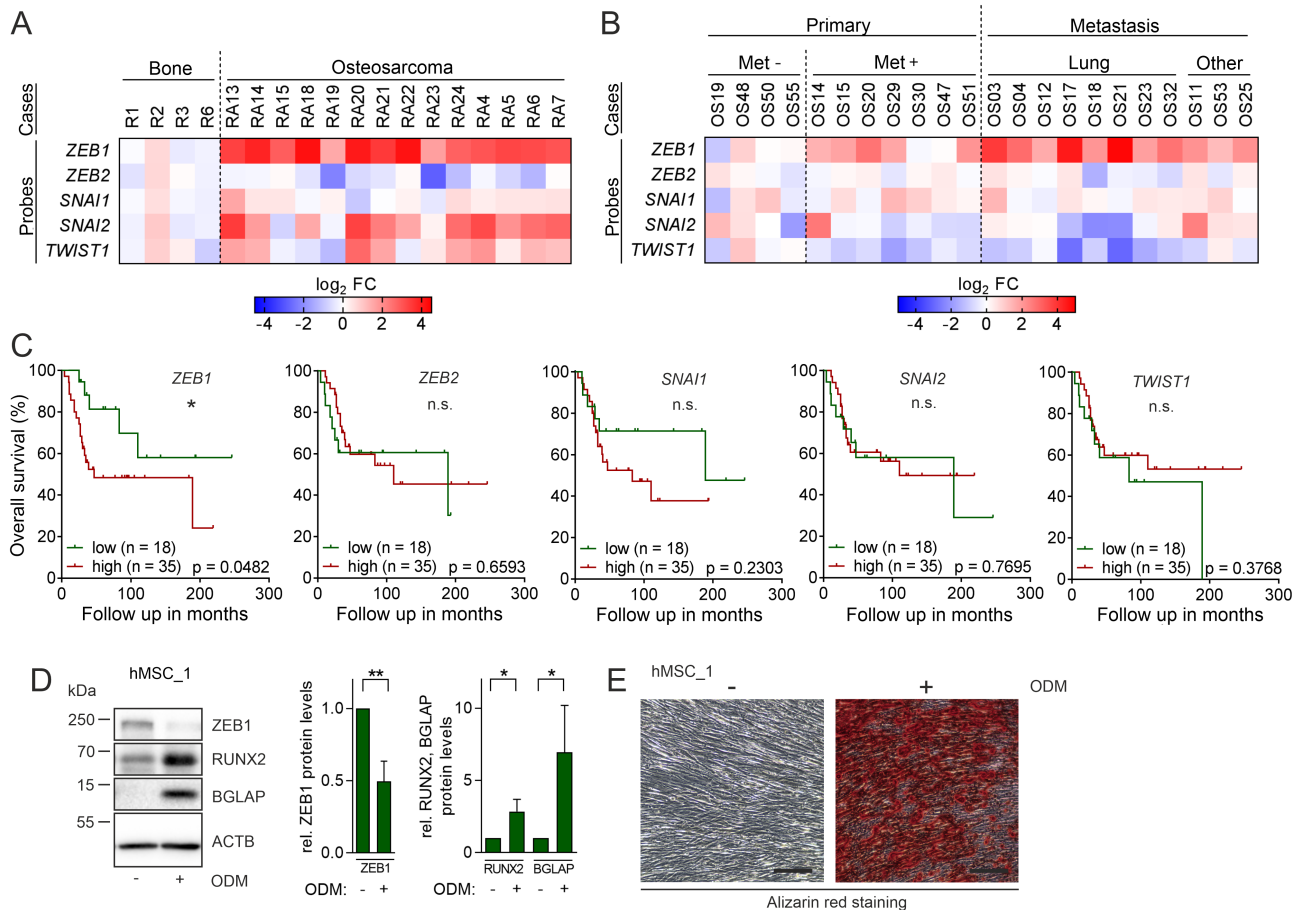
Figure 1. ZEB1 is elevated in osteosarcoma and correlates with progression and poor survival. (A) Comparative analysis of mRNA expression in human osteosarcoma tumor samples ($n = 14$) relative to normal human bone samples ($n = 4$) (E-MEXP-3628). The heat map illustrates log_2 FC values. (B) Comparative analysis of mRNA expression in human osteosarcoma tumor samples without (Met−, $n = 4$) or with (Met+, $n = 7$) detectable metastases and distant metastasis samples ($n = 11$) (GSE32981). The heat map illustrates log_2 FC values. (C) Kaplan–Meier curves showing the overall survival probability dependent on low (lower third, $n = 18$) or high (upper two-thirds, $n = 35$) expression of the corresponding EMT-TF (GSE21257); log-rank (Mantel–Cox) test. (D) Representative western blot and chemiluminescence-based protein quantification of ZEB1, RUNX2, and osteocalcin (BGLAP) in hMSC_1 cells cultured with or without osteogenic differentiation medium (ODM) for 21 days. ACTB was used as a loading control. $n = 3$, mean $\pm$ SD; Student's t-test (two-tailed). (E) Representative phase-contrast images of hMSC_1 cells used in D. Alizarin red staining at day 21. Scale bars: 200 μm.

deposits, over time also further reduced ZEB1 expression but slightly upregulated SNAIL and TWIST1 expression (Figure 1D,E and supplementary material, Figure S1D). These data indicate that among the core EMT-TFs, especially ZEB1 impacts osteosarcoma progression and prognosis. Its downregulation upon osteoblast differentiation points to a potential ZEB1-dependent pathological mechanism during osteosarcoma progression.

ZEB1 blocks osteoblastic differentiation in mesenchymal stem cells and osteosarcoma cells

Blocking osteoblastic differentiation is an important aspect of osteosarcoma progression [2]. The observation of increased ZEB1 expression in osteosarcoma cells and its strong downregulation during osteoblastic differentiation of MSCs prompted us to analyze its role in the osteoblastic lineage under physiological and pathophysiological conditions. Among many other defects, conventional *Zeb1* knockout mice display a variety of skeletal abnormalities

[30] that we could recapitulate using our published *Zeb1flox* allele [19]. Strikingly, in E15.5 *Zeb1*-deficient embryos (*Zeb1del/del*), the most severe defect was the shortening of long bones (Figure 2A and supplementary material, Figure S2A), which we hypothesized to result from premature osteoblastic differentiation. To functionally analyze the role of Zeb1 in this physiological process, we isolated MSCs from the compact bone of *Zeb1flox/flox* [19] or *R26-Zeb1tg/tg* mice [20], which can be directed to undergo osteoblastic differentiation. They displayed the typical surface marker expression of mouse MSCs (mMSCs) (supplementary material, Figure S2B) [31,32]. Adeno-Cre virus (a-Cre) transduction led to almost complete knockout (*Zeb1flox/flox*) or mild overexpression (*R26-Zeb1tg/tg* mice) of *Zeb1* (supplementary material, Figure S2C). Induction of osteoblastic differentiation in non-recombined mMSCs resulted in increased alkaline phosphatase (ALP) staining, a marker for early osteoblastic cells, after 7 days. Of note, *Zeb1*-depleted cells exhibited spontaneous strong ALP staining, even without extrinsic induction, highlighting
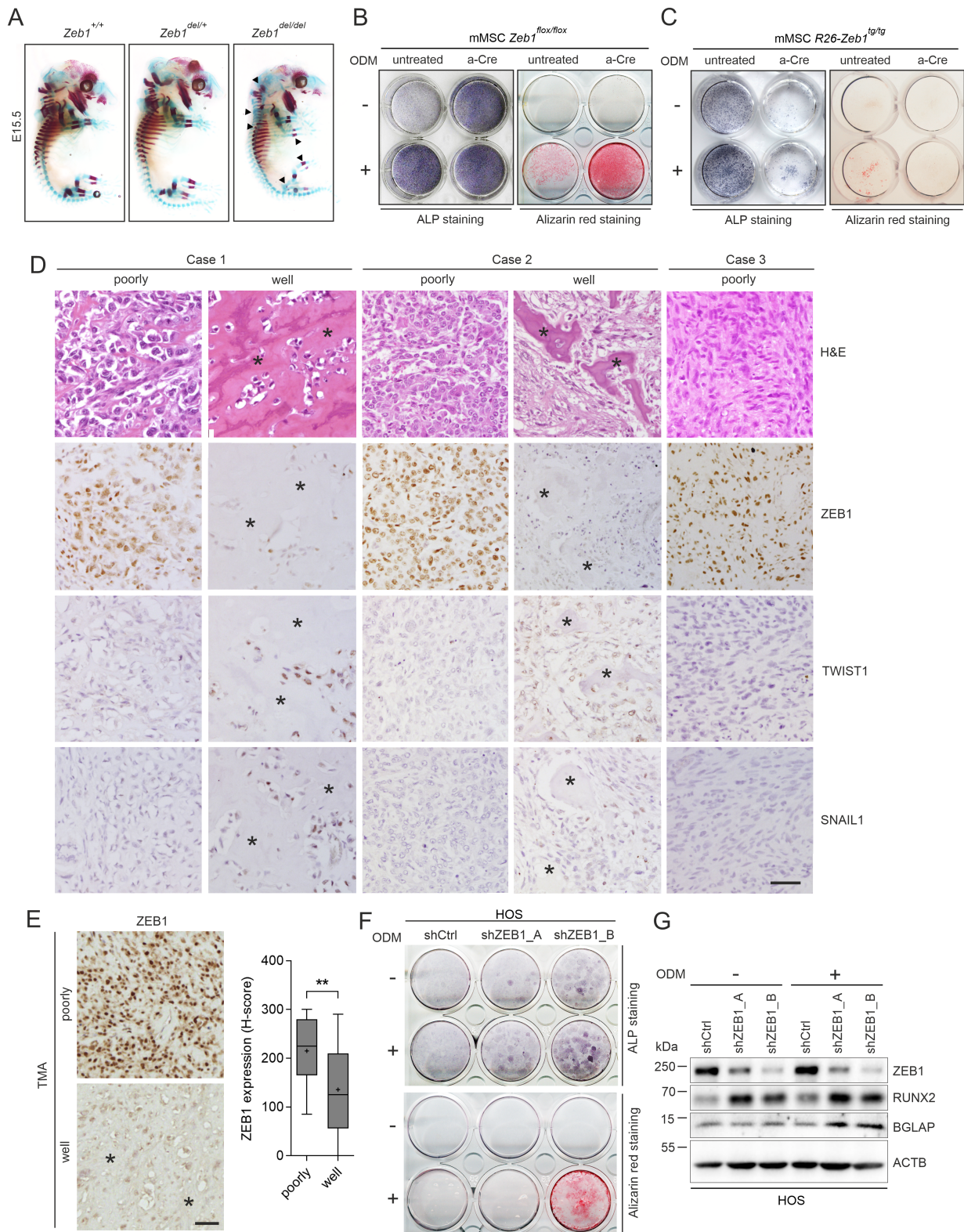
Figure 2. ZEB1 regulates osteoblastic differentiation in mesenchymal stem cells and osteosarcoma cells. (A) Representative images of Alizarin red/Alcian blue staining of the skeletons from E15.5 $Zeb1^{+/+}$ ($n = 5$), $Zeb1^{del/+}$ ($n = 3$), and $Zeb1^{del/del}$ ($n = 4$) embryos. Arrowheads mark skeletal defects. (B, C) Representative alkaline phosphatase (ALP) staining at day 7 and Alizarin red staining at day 21 of untreated and a-Cre transduced $Zeb1^{flox/flox}$ mMSCs (B) or $R26-Zeb1^{tg/tg}$ mMSCs (C) cultured with or without osteogenic differentiation medium (ODM). $n = 3$. (D) Representative images of H&E and immunohistochemical ZEB1, TWIST1, and SNAI1 staining of osteosarcoma tumors. For cases 1 and 2, a poorly differentiated and a well-differentiated area are shown. Asterisks mark osteoid deposition. Scale bar: 50 μm. (E) Example images of immunohistochemical ZEB1 staining of a well- and a poorly-differentiated tumor in the osteosarcoma tissue microarray (TMA). Asterisks mark osteoid deposition. Scale bar: 50 μm. H-scores of poorly ($n = 11$) and well ($n = 103$)-differentiated tumors. H-score is the sum of four staining intensities (0 = negative, 1 = low, 2 = medium, 3 = high) multiplied by the corresponding percentage of positive stained cells, resulting in a scale of 0–300. Box and whiskers plot: whiskers = min/max; box = 25th to 75th percentiles; middle line = median; plus = mean. Mann–Whitney test (two-tailed). (F) Representative alkaline phosphatase (ALP) staining and Alizarin red staining at day 21 of HOS cells stably transduced with shCtrl, shZEB1_A or shZEB1_B vector, cultured with or without osteogenic differentiation medium (ODM). $n = 3$. (G) Representative western blot for ZEB1, RUNX2, and osteocalcin (BGLAP) for cells used in F after 21 days. $n = 2$.

ZEB1 as a gatekeeper of osteoblastic differentiation. Furthermore, *Zeb1* knockout cells also revealed increased terminal differentiation compared with non-recombined cells, indicated by increased alizarin red staining (Figure 2B). On the other hand, Zeb1 overexpression effectively diminished osteogenic differentiation (Figure 2C). Consistent with this, we observed similar effects in human MSCs. Stable knockdown of *ZEB1* by two independent short hairpin RNAs (shRNAs) increased the proportion of ALP-positive early osteoblastic cells already without induction of osteoblastic differentiation. Of note, terminal differentiation was only increased with the more potent knockdown (shZEB1_B), indicating a dose-dependent effect (supplementary material, Figure S2D,E).

To translate these findings to the cancer context and correlate the expression of ZEB1 with the degree of differentiation in human primary osteosarcomas, we analyzed tumors which exhibited substantial intratumoral heterogeneity with poorly and well-differentiated areas in close proximity as determined by the relative number of cells compared with deposited extracellular matrix [33]. Poorly differentiated areas displayed strongly elevated ZEB1 protein levels compared with well-differentiated areas (Figure 2D). Additionally, staining of a tissue microarray (TMA) of 114 osteosarcomas also revealed increased ZEB1 expression in poorly differentiated tumors (Figure 2E). We could further support these results *in vitro* using an shRNA-mediated knockdown of *ZEB1* in human HOS osteosarcoma cells (Figure 2F). ZEB1-expressing control cells (shCtrl) were non-responsive to the osteoblastic stimulus and did not show any signs of differentiation. However, knockdown of *ZEB1* induced an early osteoblastic ALP-expressing phenotype in HOS cells already without extrinsic induction of osteoblastic differentiation, akin to the ZEB1-depleted MSCs (Figure 2B and supplementary material, Figure S2E). As seen before in the MSCs, the more potent knockdown (shZEB1_B) induced a terminal differentiation even in this aggressive osteosarcoma cell line, shown by strong Alizarin red staining (Figure 2F). Interestingly, ZEB1 could not be downregulated in HOS shCtrl cells under differentiation conditions, unlike that seen before in normal MSCs. However, shRNA-mediated depletion of ZEB1 strongly increased the expression of RUNX2, the master regulator of osteoblastic differentiation, and under differentiation conditions also led to an increase of the terminal differentiation marker osteocalcin (BGLAP) (Figure 2G).

Taken together, high ZEB1 expression inhibits osteoblastic differentiation in non-neoplastic mesenchymal stem cells and consequently prevents differentiation in osteosarcoma cells when aberrantly highly expressed, eventually locking the tumor cells in an aggressive, undifferentiated state.

ZEB1 stimulates metastatic colonization

Expression of ZEB1 in osteosarcoma cells has already been correlated with increased proliferation as well as with migration and invasion [8,34]. We established stable shRNA-mediated knockdown of *ZEB1* in different osteosarcoma cell lines, as well as moderate overexpression of *ZEB1* in the relatively low-expressing Saos-2 cells (supplementary material, Figure S3A,B), and confirmed ZEB1-dependent invasion capacity in different osteosarcoma cell lines (supplementary material, Figure S3C). Of note, in our hands, cell proliferation was not affected by *ZEB1* knockdown or overexpression (supplementary material, Figure S3D,E), which is contradictory to published data [8,9]. However, the most relevant part of clinical progression is metastasis to the lung. Here, the critical step is metastatic colonization, the seeding of colonies in the novel environment at the distant site. This colonization capacity is highly dependent on stemness, survival, and plasticity traits, which are all known to be exerted by ZEB1 [35].

Using our stable cell lines, *ZEB1* knockdown strongly reduced, whereas overexpression enhanced *in vitro* clonogenic capacity (Figure 3A,B). The same effect was seen in non-neoplastic human MSCs, in which *ZEB1* depletion completely abolished the ability to form colonies without affecting cell proliferation (supplementary material, Figure S3F,G). These data demonstrate a general function of ZEB1 in the clonal outgrowth of mesenchymal cells.

To further determine whether ZEB1 facilitates colonization and subsequent metastatic outgrowth *in vivo*, we used the highly metastatic 143B osteosarcoma cell line in an experimental metastasis assay. Tumor cells were injected into the tail vein of immunodeficient mice and the formation of macrometastases in the lung and liver was assessed after 3 weeks. *ZEB1* knockdown significantly reduced the number of metastatic colonies in the lung (Figure 3C and supplementary material, Figure S3H) and the liver (Figure 3D and supplementary material, Figure S3I).

Taken together, these data provide evidence that aberrant ZEB1 expression increases the colonization capacity and promotes metastasis formation of osteosarcoma cells.

## Loss of imprinting at the *DLK1–DIO3* locus enables indirect epigenetic targeting of ZEB1-driven osteosarcomas

Our data show that ZEB1 expression in osteosarcoma blocks differentiation and increases the metastatic colonization capacity. Since metastasis is the major cause of death for osteosarcoma patients, ZEB1 would be a candidate therapeutic target. But because transcription factors are hard to target, we focused on its upstream regulation. On the one hand, previous studies have suggested that the miR200 family, which is reciprocally linked to ZEB1 expression by a double-negative ZEB1/miR200 feedback loop in epithelial cells [36], is involved in the progression of osteosarcoma [37,38]. However, our analysis revealed that they were not differentially and were very weakly expressed in hMSCs and hOSCs (Figure 4A) and that their inhibition in hMSCs had no effect on ZEB1 expression (supplementary material, Figure S4A,B). On the other hand, there is the

imprinted *DLK1-DIO3* locus, which is dysregulated in 90% of osteosarcomas [13] and encodes a large cluster of microRNAs (Figure 4B). Their downregulation in osteosarcoma correlates with shorter overall survival and metastasis [10–12]. By analyzing the expression of the *DLK1-DIO3* miRNAs in the NCI sarcoma cell line panel [40], we could confirm substantially decreased expression levels of these miRNAs in osteosarcoma cell lines compared with normal human non-neoplastic connective tissue cells or other sarcoma subtypes (Figure 4C). 73% of the *DLK1-DIO3* encoded microRNAs are supposed to target ZEB1 (Figure 4D). RT-qPCR confirmed the downregulation of the top six ZEB1-targeting of these microRNAs (calculated by three different microRNA target prediction tools) in osteosarcoma cell lines compared with hMSCs (Figure 4E).

Overexpression of silenced individual or particularly the combination of the top six *DLK1-DIO3* encoded microRNAs reduced ZEB1 expression to a similar extent to our positive control, MIR200c (Figure 4F). Moreover, combined downregulation of only three endogenous microRNAs of the cluster, namely MIR409-3p, MIR431-3p, and MIR655-3p, in hMSCs by anti-MIRs led to increased ZEB1 expression (Figure 4G,H). Interestingly, these three miRNAs have

already been linked to ZEB1 suppression [8,16,18]. We could confirm that they directly targeted *ZEB1* 3'-UTR in luciferase reporter assays, where transfection of *pre-MIR431-5p*, *pre-MIR409-3p*, and *pre-MIR655-3p* significantly reduced the luciferase activity, while mutation of their respective seed sequences resulted in a complete rescue (supplementary material, Figure S4C–F).

Next, we wanted to test if a pharmacologic reactivation of silenced endogenous microRNAs encoded in *DLK1-DIO3*, which should lead to ZEB1 repression, was feasible. Apart from the miRNAs, the imprinted locus also contains three long non-coding RNAs (lncRNAs): *MEG3*, *MEG8*, and *MEG9*. The *DLK1-DIO3* locus is tightly regulated by two differently methylated imprinting control regions (IG-DMR, MEG3-DMR). Hypermethylation of the MEG3-DMR is associated with reduced expression of the maternally expressed non-coding RNAs [41,42]. Using a methylation-specific PCR [23] (Figure 5A), we observed that all hMSCs showed the predicted equal amount of unmethylated and methylated PCR product, whereas we detected a reduction in the unmethylated PCR product in three out of five hOSCs (Figure 5B), fitting with the silencing of the microRNAs. Treatment of hOSCs with the demethylating agent 5-aza-2'-deoxycytidine (5-Aza) resulted
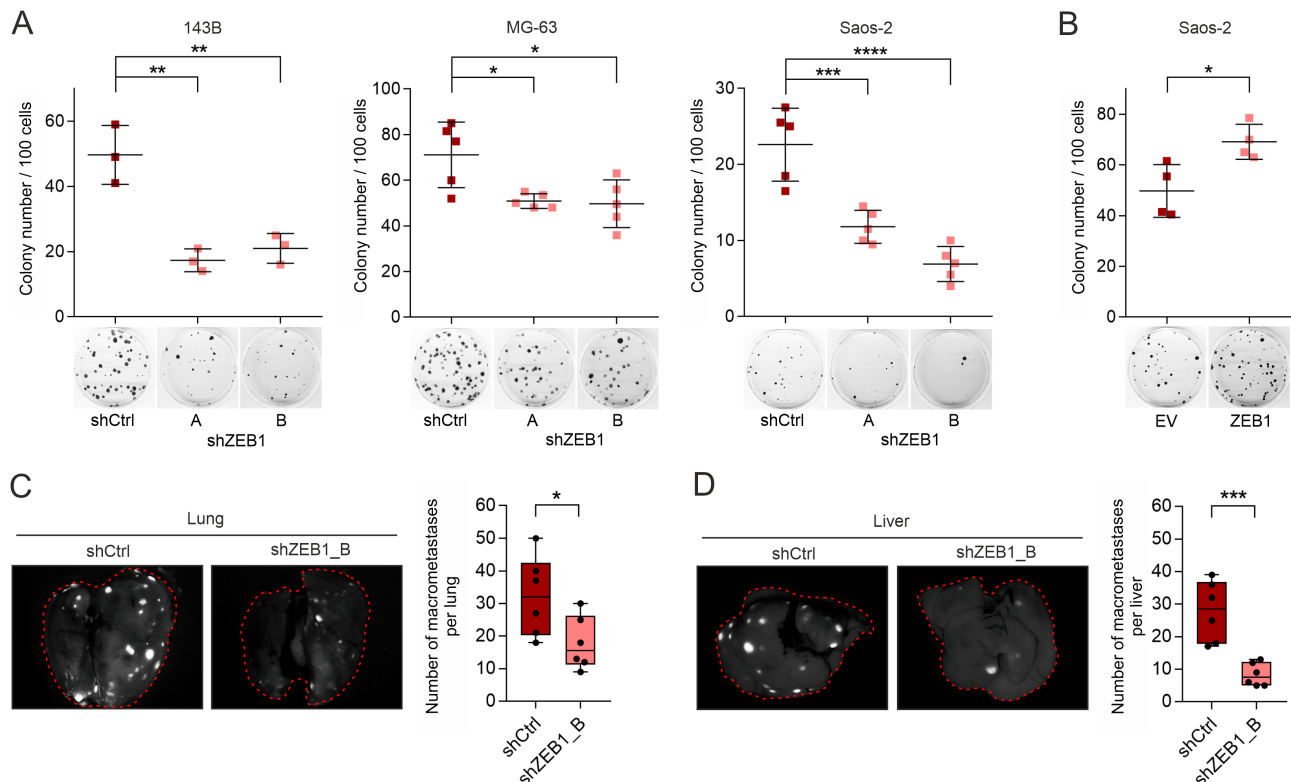
Figure 3. ZEB1 facilitates tumorigenic traits of osteosarcoma cells *in vitro* and *in vivo*. (A) Representative images and quantification of colony formation assays with 143B (8 days), MG-63 (14 days), and Saos-2 (21 days) cells stably transduced with shCtrl, shZEB1_A or shZEB1_B vector. $n = 3$ (143B), $n = 5$ (MG-63, Saos-2), mean $\pm$ SD; one-way ANOVA with correction for multiple comparisons using the Dunnett method. (B) Representative images and quantification of colony formation assays with Saos-2 cells (21 days) stably transduced with empty vector (EV) or HA-tagged ZEB1 (ZEB1 OE). $n = 4$, mean $\pm$ SD; Student's *t*-test (two-tailed). (C, D) *Ex vivo* GFP–fluorescence imaging and quantification of macrometastases per lung (C) and liver (D) 3 weeks after injection of 1×10^5 143B cells into the lateral tail vein of immunodeficient NSG mice: shCtrl ($n = 6$) or shZEB1_B ($n = 6$). Representative overview pictures of the liver are assembled out of four individual images. Mean $\pm$ SD; Student's *t*-test (two-tailed).
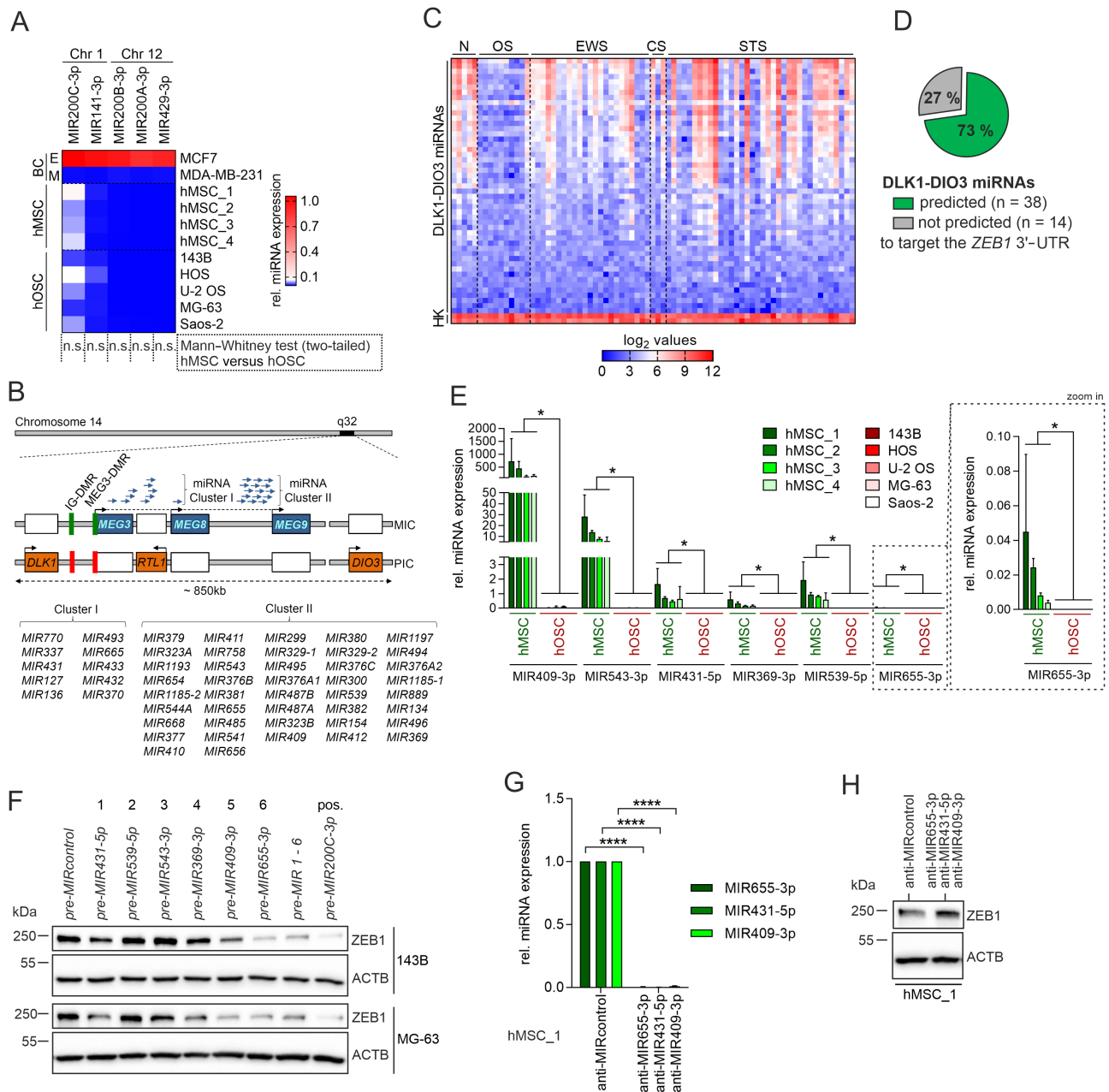
Figure 4. Loss of miRNAs encoded by the imprinted *DLK1-DIO3* locus drives ZEB1 overexpression in osteosarcoma. (A) RT-qPCR analysis of the miRNA-200 family members on chromosome (Chr) 1 and Chr 12. The heat map illustrates the expression values of hMSCs and hOSCs relative to epithelial 'E' MCF7 and mesenchymal-like 'M' MDA-MB-231 breast carcinoma cell lines. *n* = 3, mean (SD is not depicted). Statistical comparison of hMSCs versus hOSCs: Mann–Whitney test (two-tailed). (B) Schematic representation of the *DLK1-DIO3* locus on human chromosome 14q32. The lncRNAs (*MEG3, MEG8,* and *MEG9*), miRNAs, and snoRNAs (not depicted) are expressed from the maternally inherited chromosome and the protein-coding genes (*DLK1, RTL1,* and *DIO3*) from the paternally inherited chromosome. Open boxes represent repressed genes. The imprinting status is determined by two differentially methylated regions (DMRs), the intergenic DMR (IG-DMR) and the MEG3-DMR (green = unmethylated; red = methylated). All miRNAs of the locus are depicted and classified into two sub-clusters. Adapted from [39]. (C) Comparative expression analysis of miRNAs located in the *DLK1-DIO3* locus. The GSE69524 data set was used, comparing human sarcoma cell lines relative to human non-neoplastic connective tissue cell lines. The heat map illustrates $\log_2$ values. *N* = human non-neoplastic connective tissue cells (*n* = 5); OS = human osteosarcoma cell lines (*n* = 10); EWS = human Ewing's sarcoma cell lines (*n* = 23); CS = human chondrosarcoma cell lines (*n* = 3); STS = human soft tissue sarcoma cell lines (*n* = 36); HK = 'housekeeping' genes (MIR16-5p and MIR191-5p). (D) Number of *DLK1-DIO3* miRNAs that are predicted to target the *ZEB1* 3'-UTR by at least one of three online miRNA target prediction programs (TargetScan, miRanda, and miRDB). (E) RT-qPCR analysis of miRNAs in hMSCs and hOSCs. *n* = 3, mean ± SD; Mann–Whitney test (two-tailed). (F) Representative western blots of 143B and MG-63 cells transfected with the indicated pre-miRNAs for 24 h. ACTB was used as a loading control. pos. = positive control; *n* = 3. (G) RT-qPCR analysis of miRNAs in hMSC_1 cells transfected with anti-MIRcontrol or anti-MIR431-5p/anti-MIR409-3p/anti-MIR655-3p miRNA inhibitors for 72 h. *n* = 3, mean ± SD; Student's *t*-test (two-tailed). (H) Representative western blot for ZEB1 in hMSC_1 cells used in G. *n* = 3.

in the re-expression of *MEG3*, *MEG8*, and *MEG9*, as well as MIR409-3p and MIR431-5p, representing both miRNA sub-clusters in the *DLK1-DIO3* locus (Figure 5C). Reciprocally, 5-Aza treatment downregulated ZEB1 protein levels in 143B, HOS, and Saos-2 cells (Figure 5D).
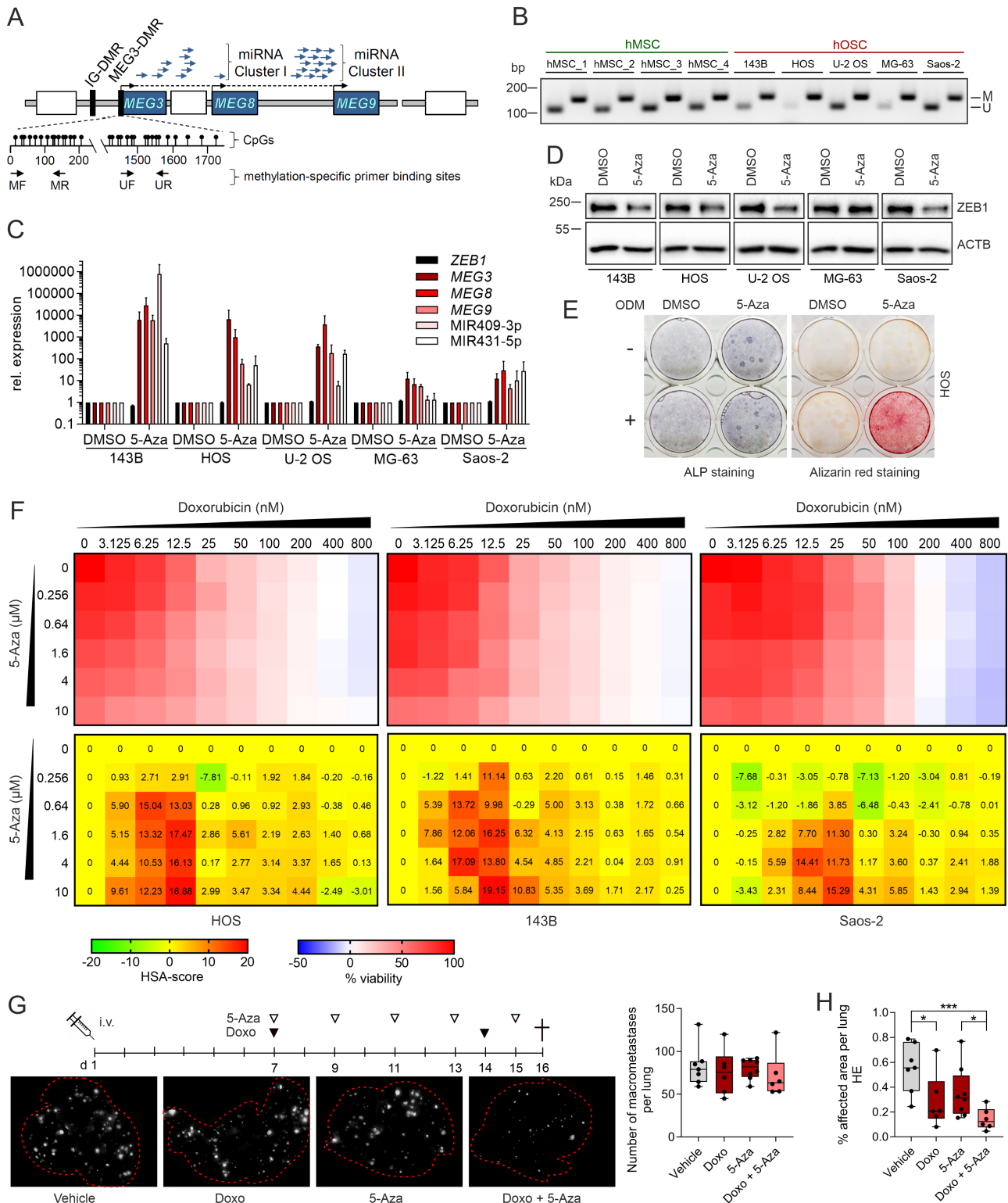
Figure 5. Loss of imprinting at the *DLK1–DIO3* locus enables indirect epigenetic targeting of ZEB1-driven osteosarcomas. (A) Schematic representation of primer binding sites for the methylation-specific PCR of the MEG3-DMR. Adapted from [23]. (B) Methylation-specific PCR screen of bisulfite-treated genomic DNA of hMSCs and hOSCs with primers shown in A. M = PCR product of methylated-DNA specific primers (160 bp); U = PCR product of unmethylated-DNA specific primers (120 bp). (C) RT-qPCR analysis of miRNAs, lncRNAs, and *ZEB1* in hOSCs treated with 5-aza-2′-deoxycytidine (5-Aza) for 72 h. Dimethyl sulfoxide (DMSO) was used as a vehicle treatment control. $n = 3$, mean $\pm$ SD. (D) Western blot analysis for ZEB1 of cells used in C. ACTB was used as a loading control. $n = 3$. (E) Representative alkaline phosphatase (ALP) staining at day 14 and Alizarin red staining at day 21 of HOS cells cultured with or without osteogenic differentiation medium (ODM) and treated with 5-Aza or DMSO for the indicated time. $n = 3$. (F) Top: dose–response matrix of 5-Aza and doxorubicin in HOS, 143B, and Saos-2 cells. Bottom: excess over highest single agent (HSA) matrix. $n = 2$. (G) *Ex vivo* GFP-fluorescence imaging and quantification of macrometastases per lung 16 days after injection of 2×10^5 143B cells into the tail vein of NSG mice: vehicle ($n = 7$), Doxo ($n = 6$), 5-Aza ($n = 8$) or Doxo + 5-Aza ($n = 7$) was administered i.p. as depicted. Mean $\pm$ SD. (H) Quantification of metastasis-affected lung area from H&E staining of two representative sections (distance 200 μm) per lung using ImageJ. Mean $\pm$ SD; unpaired Student's *t*-test.

Poorly differentiated osteosarcomas show a much higher risk of developing metastases and local recurrence than well-differentiated tumors [33,43]. This is further underlined by *in vitro* studies showing that osteoblastic differentiation in osteosarcoma cells reduces their malignant potential [44,45]. Thus, we tested if reactivation of hypermethylated *DLK1-DIO3* miRNA genes would induce osteoblastic differentiation similar to an artificial downregulation of ZEB1. Indeed, 5-Aza-treated HOS cells exhibited a higher proportion of ALP-positive early osteoblastic cells and strong induction of terminal differentiation under differentiation conditions, demonstrated by distinct Alizarin red S staining (Figure 5E), similar to a *ZEB1* knockdown in these cells (compare Figure 2F). Since in carcinoma, expression of EMT-TFs is strongly associated with a drug resistance phenotype [3,35], we determined whether 5-Aza treatment of osteosarcoma cells also increases sensitivity to standard chemotherapeutic drugs, such as doxorubicin. Using a dose–response matrix of 45 different combinations of 5-Aza and doxorubicin dose levels, we detected an excess over the highest single agent response (HSA) at low doxorubicin concentrations in different osteosarcoma cell lines (Figure 5F). To confirm these results *in vivo*, we injected 143B cells i.v. and allowed metastasis formation for 1 week before starting treatment with vehicle, doxorubicin, 5-Aza or a combination. As expected, all groups developed similar numbers of lung metastases, but 9 days of treatment led to a significant reduction in tumor size. Notably, the combination of doxorubicin and 5-Aza exerted the strongest inhibitory effect also *in vivo* (Figure 5G,H and supplementary material, Figure S5A,B). Therefore, a combination of 5-Aza with the standard chemotherapeutic treatment regimen might be a promising option for osteosarcoma therapy by inducing differentiation and increasing sensitivity to standard chemotherapy.

Discussion

The functional relevance of EMT-TFs in the progression of a variety of carcinomas is well known [35,46,47]. However, their function in sarcomas is only just emerging. We show here that of all core EMT-TFs, only ZEB1 was strongly elevated in primary osteosarcomas and its high expression was associated with poor clinical outcome. Furthermore, we demonstrated a crucial role of ZEB1 for maintaining an undifferentiated state in MSCs and osteosarcoma cells. ZEB1 is critical for the colonization capacity of osteosarcoma cells, which likely explains its association with poor prognosis and metastasis in patients [34]. We could confirm a direct link between aberrantly high ZEB1 expression and the well-described dysregulation of imprinted *DLK1-DIO3* miRNA genes in osteosarcoma. Their reactivation by epigenetic drugs led to downregulation of ZEB1, facilitated differentiation, and increased sensitivity to standard chemotherapy *in vitro* and *in vivo*, indicating a promising therapeutic option for fatal osteosarcomas.

Why does ZEB1 play such a prominent role in osteosarcoma? Our data demonstrate that regulated expression of ZEB1 is important for physiological bone development and homeostasis. We detected several bone defects in *Zeb1*-deficient mice, in particular a shortening of long bones. In part, these bone defects can be explained by alterations in the proliferation and patterning of chondrocytes in the growth plate of *Zeb1*-depleted mice [48]. However, our *in vitro* data using isolated MSCs provide evidence that ZEB1 also plays an important role in controlling the differentiation of osteoblasts. We showed that ZEB1 is markedly downregulated during osteoblastic differentiation and its depletion results in a premature differentiation of MSCs, which might also explain the observed shortening of long bones. Strikingly, different EMT-TFs seem to play different roles in osteoblastic differentiation. Similar to Zeb1, Twist1 overexpression inhibits osteoblastic differentiation [49]; however, we found Twist1 to be only weakly expressed in hMSCs and not considerably regulated upon osteogenic differentiation. Further, it seems not to be relevant in osteosarcoma, as we did not detect any overexpression. In contrast to ZEB1, Weiss and coworkers showed that a double knockout of *Snai1* and *Snai2* in MSCs results in suppression of terminal osteoblastic differentiation [50,51]. These data underscore the non-redundant and partially opposing functions of EMT-TFs [35,47] and indicate why ZEB1 particularly plays a crucial role in osteosarcoma. Indeed, we found that ZEB1 is significantly more highly expressed in poorly differentiated human osteosarcomas compared with more differentiated subtypes.

Many osteosarcoma cell lines have lost the ability to undergo osteoblastic differentiation [52]. We showed that ZEB1 depletion in differentiation-incompetent HOS cells renders them susceptible to a differentiation stimulus until terminal differentiation. Of note, our data provide evidence that a ZEB1-mediated repression of RUNX2 causes the block of osteoblastic differentiation in these cells. Besides the inhibition of osteoblastic differentiation, we also demonstrated that ZEB1 promotes clonal growth and consequently metastatic colonization of osteosarcoma cells. This is of utmost importance, as early spread of tumor cells is the major obstacle in the treatment of osteosarcoma patients. It is considered that undetectable micrometastases are present in the lungs of about 80% of patients at the time of diagnosis [53], which drops the survival rate from approximately 70% in patients with localized disease down to 20% in patients with metastatic or relapsed tumors [54]. In summary, our findings support the view that osteosarcoma formation and progression are driven by impaired osteoblastic differentiation and indicate that elevated expression of ZEB1 is an important molecular cause by blocking osteoblastic differentiation and keeping tumor cells in an undifferentiated aggressive state.

The imprinted *DLK1-DIO3* locus represents the largest miRNA cluster in mammals, including 52 different miRNAs [14] with mostly unknown physiological role. The deregulation of some *DLK1-DIO3* encoded miRNAs is associated with the progression of several tumor

entities such as squamous cell carcinoma, gastrointestinal cancer, and glioma [55]. Strikingly, in almost 90% of osteosarcoma patients younger than 30 years, the *DLK1-DIO3* locus exhibits imprinting defects and down-regulation of the encoded miRNAs correlates with shorter overall survival and metastasis [10–13]. Our *in silico* analysis predicted *ZEB1* as a target of the majority of the 52 *DLK1-DIO3* miRNAs. The redundancy of these miR-NAs in limiting the expression of ZEB1 indicates an important role of the *DLK1-DIO3* cluster in regulating and fine tuning ZEB1 expression. Besides ZEB1, *DLK1-DIO3* miRNAs were also shown to repress other osteosarcoma driver genes, such as *YBX1* and *MYC*, altogether demonstrating the important tumor-suppressive role of the locus in this tumor entity [12,56].

Our data indicate that hypermethylation of the imprinted *DLK1-DIO3* locus is likely the major reason for the lost miRNA expression in osteosarcoma. Instantly, the aberrant hypermethylation of the *DLK1-DIO3* locus paves the way for a potential therapeutic intervention. Due to the lack of specific inhibitors of ZEB1, the epigenetic reactivation of the *DLK1-DIO3* miRNAs by the FDA-approved drug 5-Aza may represent an applicable way to control the aberrant expression of ZEB1 in osteosarcoma but also of other associated driver factors, such as MYC. We demonstrated that 5-Aza treatment induces terminal differentiation of osteosarcoma cells, at least in part due to the *DLK1-DIO3* miRNA-mediated downregulation of ZEB1. Efficient treatment of osteosarcoma by demethylation with 5-Aza was recently demonstrated in a mouse xenograft model [57]. However, based on the pleiotropic effects of epigenetic drugs, it is likely that the regulation of other factors is also involved in this process. Clinically relevant, our data further indicate a synergistic effect in inhibiting metastatic growth using a combination of 5-Aza and the standard chemotherapeutic doxorubicin.

In summary, we have characterized here the important role of ZEB1 in controlling both osteoblastic differentiation and the formation and progression of osteosarcoma. Furthermore, our findings highlight a therapeutic option for this fatal disease.

Acknowledgements

Author contributions statement

MRu planned and carried out experiments and wrote the manuscript. MPS, IF, KF, JK, RvR and MRo carried out experiments. HS and RE gave critical input to the manuscript. GB provided the *R26-Zeb1^{tg/tg}* mouse strain. FM provided NSG mice and co-planned grafting experiments. DB acquired and provided the tissue microarray. AA acquired and provided clinical samples. MPS, SB and TB supervised, planned experiments, and wrote and reviewed the manuscript.

References

1. Bacci G, Ferrari S, Longhi A, *et al*. Pattern of relapse in patients with osteosarcoma of the extremities treated with neoadjuvant chemotherapy. *Eur J Cancer* 2001; **37:** 32–38.

2. Wagner ER, Luther G, Zhu G, *et al*. Defective osteogenic differentiation in the development of osteosarcoma. *Sarcoma* 2011; **2011:** 325238.

3. Nieto MA, Huang RY, Jackson RA, *et al*. EMT: 2016. *Cell* 2016; **166:** 21–45.

4. Yang J, Antin P, Berx G, *et al*. Guidelines and definitions for research on epithelial–mesenchymal transition. *Nat Rev Mol Cell Biol* 2020; **21:** 341–352.

5. Feng T, Zhu Z, Jin Y, *et al*. The microRNA-708-5p/ZEB1/EMT axis mediates the metastatic potential of osteosarcoma. *Oncol Rep* 2020; **43:** 491–502.

6. Jiang R, Zhang C, Liu G, *et al*. MicroRNA-126 inhibits proliferation, migration, invasion, and EMT in osteosarcoma by targeting ZEB1. *J Cell Biochem* 2017; **118:** 3765–3774.

7. Wang H, Xing D, Ren D, *et al*. MicroRNA-643 regulates the expression of ZEB1 and inhibits tumorigenesis in osteosarcoma. *Mol Med Rep* 2017; **16:** 5157–5164.

8. Wu L, Zhang Y, Huang Z, *et al*. MiR-409-3p inhibits cell proliferation and invasion of osteosarcoma by targeting zinc-finger E-box-binding homeobox-1. *Front Pharmacol* 2019; **10:** 137.

9. Zhu C, Cheng D, Qiu X, *et al*. Long noncoding RNA SNHG16 promotes cell proliferation by sponging microRNA-205 and upregulating ZEB1 expression in osteosarcoma. *Cell Physiol Biochem* 2018; **51:** 429–440.

10. Maire G, Martin JW, Yoshimoto M, *et al*. Analysis of miRNA-gene expression-genomic profiles reveals complex mechanisms of microRNA deregulation in osteosarcoma. *Cancer Genet* 2011; **204:** 138–146.

11. Sarver AL, Thayanithy V, Scott MC, *et al*. MicroRNAs at the human 14q32 locus have prognostic significance in osteosarcoma. *Orphanet J Rare Dis* 2013; **8:** 7.

12. Thayanithy V, Sarver AL, Kartha RV, *et al*. Perturbation of 14q32 miRNAs-cMYC gene network in osteosarcoma. *Bone* 2012; **50:** 171–181.

13. Shu J, Li L, Sarver AE, *et al*. Imprinting defects at human 14q32 locus alters gene expression and is associated with the pathobiology of osteosarcoma. *Oncotarget* 2016; **7:** 21298–21314.

14. da Rocha ST, Edwards CA, Ito M, *et al*. Genomic imprinting at the mammalian *Dlk1-Dio3* domain. *Trends Genet* 2008; **24:** 306–316.

15. Haga CL, Phinney DG. MicroRNAs in the imprinted *DLK1-DIO3* region repress the epithelial-to-mesenchymal transition by targeting the TWIST1 protein signaling network. *J Biol Chem* 2012; **287:** 42695–42707.

16. Harazono Y, Muramatsu T, Endo H, *et al*. miR-655 is an EMT-suppressive microRNA targeting ZEB1 and TGFBR2. *PLoS One* 2013; **8:** e62757.

17. Ma Z, Li Y, Xu J, *et al*. MicroRNA-409-3p regulates cell invasion and metastasis by targeting ZEB1 in breast cancer. *IUBMB Life* 2016; **68:** 394–402.

18. Sun K, Zeng T, Huang D, *et al*. MicroRNA-431 inhibits migration and invasion of hepatocellular carcinoma cells by targeting the ZEB1-mediated epithelial–mensenchymal transition. *FEBS Open Bio* 2015; **5:** 900–907.

19. Brabletz S, Lasierra Losada M, Schmalhofer O, *et al*. Generation and characterization of mice for conditional inactivation of Zeb1. *Genesis* 2017; **55.**

20. Goossens S, Wang J, Tremblay CS, *et al*. ZEB2 and LMO2 drive immature T-cell lymphoblastic leukemia via distinct oncogenic mechanisms. *Haematologica* 2019; **104:** 1608–1616.

21. Bedzhov I, Alotaibi H, Basilicata MF, *et al*. Adhesion, but not a specific cadherin code, is indispensable for ES cell and induced pluripotency. *Stem Cell Res* 2013; **11:** 1250–1263.

22. Krützfeldt J, Kuwajima S, Braich R, *et al*. Specificity, duplex degradation and subcellular localization of antagomirs. *Nucleic Acids Res* 2007; **35:** 2885–2892.

23. Murphy SK, Wylie AA, Coveler KJ, *et al*. Epigenetic detection of human chromosome 14 uniparental disomy. *Hum Mutat* 2003; **22:** 92–97.

24. Hayashi S, Lewis P, Pevny L, *et al*. Efficient gene modulation in mouse epiblast using a *Sox2Cre* transgenic mouse strain. *Mech Dev* 2002; **119**(Suppl 1): S97–S101.

25. Krebs AM, Mitschke J, Lasierra Losada M, *et al*. The EMT-activator Zeb1 is a key factor for cell plasticity and promotes metastasis in pancreatic cancer. *Nat Cell Biol* 2017; **19:** 518–529.

26. Namløs HM, Kresse SH, Müller CR, *et al*. Global gene expression profiling of human osteosarcomas reveals metastasis-associated chemokine pattern. *Sarcoma* 2012; **2012:** 639038.

27. Betel D, Wilson M, Gabow A, *et al*. The microRNA.org resource: targets and expression. *Nucleic Acids Res* 2008; **36**(Database issue): D149–D153.

28. Quist T, Jin H, Zhu JF, *et al*. The impact of osteoblastic differentiation on osteosarcomagenesis in the mouse. *Oncogene* 2015; **34:** 4278–4284.

29. Mutsaers AJ, Walkley CR. Cells of origin in osteosarcoma: mesenchymal stem cells or osteoblast committed cells? *Bone* 2014; **62:** 56–63.

30. Takagi T, Moribe H, Kondoh H, *et al*. DeltaEF1, a zinc finger and homeodomain transcription factor, is required for skeleton patterning in multiple lineages. *Development* 1998; **125:** 21–31.

31. Houlihan DD, Mabuchi Y, Morikawa S, *et al*. Isolation of mouse mesenchymal stem cells on the basis of expression of Sca-1 and PDGFR-alpha. *Nat Protoc* 2012; **7:** 2103–2111.

32. Zhu H, Guo ZK, Jiang XX, *et al*. A protocol for isolation and culture of mesenchymal stem cells from mouse compact bone. *Nat Protoc* 2010; **5:** 550–560.

33. Fletcher CDM, Unni KK, Mertens F. *Pathology and Genetics of Tumours of Soft Tissue and Bone (World Health Organization Classification of Tumours)*. WHO, IARC Press: Lyon, 2002.

34. Shen A, Zhang Y, Yang H, *et al*. Overexpression of ZEB1 relates to metastasis and invasion in osteosarcoma. *J Surg Oncol* 2012; **105:** 830–834.

35. Stemmler MP, Eccles RL, Brabletz S, *et al*. Non-redundant functions of EMT transcription factors. *Nat Cell Biol* 2019; **21:** 102–112.

36. Brabletz S, Brabletz T. The ZEB/miR-200 feedback loop – a motor of cellular plasticity in development and cancer? *EMBO Rep* 2010; **11:** 670–677.

37. Liu X, Liu Y, Wu S, *et al*. Tumor-suppressing effects of miR-429 on human osteosarcoma. *Cell Biochem Biophys* 2014; **70:** 215–224.

38. Xu H, Mei Q, Xiong C, *et al*. Tumor-suppressing effects of miR-141 in human osteosarcoma. *Cell Biochem Biophys* 2014; **69:** 319–325.

39. Das PP, Hendrix DA, Apostolou E, *et al*. PRC2 is required to maintain expression of the maternal *Gtl2-Rian-Mirg* locus by preventing *de novo* DNA methylation in mouse embryonic stem cells. *Cell Rep* 2015; **12:** 1456–1470.

40. Teicher BA, Polley E, Kunkel M, *et al*. Sarcoma cell line screen of oncology drugs and investigational agents identifies patterns associated with gene and microRNA expression. *Mol Cancer Ther* 2015; **14:** 2452–2462.

41. Kagami M, O'Sullivan MJ, Green AJ, *et al*. The IG-DMR and the *MEG3*-DMR at human chromosome 14q32.2: hierarchical interaction and distinct functional properties as imprinting control centers. *PLoS Genet* 2010; **6:** e1000992.

42. Kameswaran V, Bramswig NC, McKenna LB, *et al*. Epigenetic regulation of the DLK1-MEG3 microRNA cluster in human type 2 diabetic islets. *Cell Metab* 2014; **19:** 135–145.

43. Clark JC, Dass CR, Choong PF. A review of clinical and molecular prognostic factors in osteosarcoma. *J Cancer Res Clin Oncol* 2008; **134:** 281–297.

44. Luo P, Yang X, Ying M, *et al*. Retinoid-suppressed phosphorylation of RARalpha mediates the differentiation pathway of osteosarcoma cells. *Oncogene* 2010; **29:** 2772–2783.

45. Sciandra M, Marino MT, Manara MC, *et al*. CD99 drives terminal differentiation of osteosarcoma cells by acting as a spatial regulator of ERK 1/2. *J Bone Miner Res* 2014; **29:** 1295–1309.

46. Sánchez-Tilló E, Liu Y, de Barrios O, *et al*. EMT-activating transcription factors in cancer: beyond EMT and tumor invasiveness. *Cell Mol Life Sci* 2012; **69:** 3429–3456.

47. Puisieux A, Brabletz T, Caramel J. Oncogenic roles of EMT-inducing transcription factors. *Nat Cell Biol* 2014; **16:** 488–494.

48. Bellon E, Luyten FP, Tylzanowski P. delta-EF1 is a negative regulator of Ihh in the developing growth plate. *J Cell Biol* 2009; **187:** 685–699.

49. Bialek P, Kern B, Yang X, *et al*. A twist code determines the onset of osteoblast differentiation. *Dev Cell* 2004; **6:** 423–435.

50. Tang Y, Weiss SJ. Snail/Slug-YAP/TAZ complexes cooperatively regulate mesenchymal stem cell function and bone formation. *Cell Cycle* 2017; **16:** 399–405.

51. Tang Y, Feinberg T, Keller ET, *et al*. Snail/Slug binding interactions with YAP/TAZ control skeletal stem cell self-renewal and differentiation. *Nat Cell Biol* 2016; **18:** 917–929.

52. Vijayakumar S, Liu G, Rus IA, *et al*. High-frequency canonical Wnt activation in multiple sarcoma subtypes drives proliferation through a TCF/β-catenin target gene, *CDC25A*. *Cancer Cell* 2011; **19:** 601–612.

53. Jaffe N. Osteosarcoma: review of the past, impact on the future. The American experience. *Cancer Treat Res* 2009; **152:** 239–262.

54. Mirabello L, Troisi RJ, Savage SA. Osteosarcoma incidence and survival rates from 1973 to 2004: data from the Surveillance, Epidemiology, and End Results Program. *Cancer* 2009; **115:** 1531–1543.

55. Benetatos L, Hatzimichael E, Londin E, *et al*. The microRNAs within the DLK1-DIO3 genomic region: involvement in disease pathogenesis. *Cell Mol Life Sci* 2013; **70:** 795–814.

56. Xu M, Jin H, Xu CX, *et al*. miR-382 inhibits osteosarcoma metastasis and relapse by targeting Y box-binding protein 1. *Mol Ther* 2015; **23:** 89–98.

57. Lillo Osuna MA, Garcia-Lopez J, El Ayachi I, *et al*. Activation of estrogen receptor alpha by decitabine inhibits osteosarcoma growth and metastasis. *Cancer Res* 2019; **79:** 1054–1068.

58. Hampf M, Gossen M. A protocol for combined *Photinus* and *Renilla* luciferase quantification compatible with protein assays. *Anal Biochem* 2006; **356:** 94–99.

Reference 58 is cited only in the supplementary material.

SUPPLEMENTARY MATERIAL ONLINE

Supplementary materials and methods

Figure S1. ZEB1 is elevated in osteosarcoma and correlates with progression and poor survival

Figure S2. ZEB1 regulates osteoblastic differentiation in mesenchymal stem cells and in osteosarcoma cells

Figure S3. ZEB1 facilitates tumorigenic traits of osteosarcoma cells *in vitro* and *in vivo*

Figure S4. ZEB1 expression is linked to the frequently inactivated *DLK1–DIO3* locus in osteosarcoma

Figure S5. Loss of imprinting at the *DLK1–DIO3* locus enables indirect epigenetic targeting of ZEB1-driven osteosarcomas

Table S1. pre-miRNAs and miRNA inhibitors

Table S2. Oligonucleotides used

Table S3. Plasmids and constructs used